

## Original Article

# Contrast-enhanced MRI and CT in evaluating treatment response for recurrent endometrial cancer: a retrospective case-control study

Yan Chen<sup>1</sup>, Xueling Wang<sup>2</sup>

<sup>1</sup>Department of Obstetrics and Gynecology, Putuo Hospital Affiliated to Shanghai University of Traditional Chinese Medicine, Shanghai 201203, China; <sup>2</sup>Department of Imaging, Yantaishan Hospital, Yantai 264001, Shandong, China

Received December 25, 2024; Accepted May 15, 2025; Epub May 15, 2025; Published May 30, 2025

**Abstract:** Objectives: To compare the diagnostic performance of contrast-enhanced magnetic resonance imaging (CE-MRI) and computed tomography (CT) in evaluating treatment response for recurrent endometrial cancer (EC), and to assess the added value of integrating imaging findings with biomarker data. Methods: This retrospective case-control study included 217 patients with recurrent EC treated between January 2020 and December 2023. Patients were divided into response (n = 102) and non-response (n = 115) based on Response Evaluation Criteria in Solid Tumors (RECIST) (1.1). An internal validation cohort (n = 142) and an external cohort (n = 168) were also analyzed. Preoperative CE-MRI and CT scans were reviewed by experienced radiologists. Biomarker positivity rates - including estrogen receptor (ER), progesterone receptor (PR), cancer antigen 125 (CA125), cancer antigen 19-9 (CA19-9), carcinoembryonic antigen (CEA), and ovarian cancer-related protein 1 (OVX1), were assessed. Multivariate logistic regression and receiver operating characteristic (ROC) analyses were performed to evaluate diagnostic performance, and an integrated model combining imaging and biomarkers was developed. Results: CE-MRI achieved an AUC of 0.864, sensitivity of 78.3%, and specificity of 86.3%, while CT showed an AUC of 0.854, sensitivity of 81.2%, and specificity of 83.4%. The integrated model improved performance with an AUC of 0.889, sensitivity of 94.3%, and specificity of 81.2%. Internal and external validation models yielded AUCs of 0.859 and 0.918, respectively. Conclusions: Both CE-MRI and CT are effective in assessing treatment response, with CE-MRI offering slightly superior specificity. Integration of imaging and biomarker data significantly enhances diagnostic accuracy, supporting its potential in optimizing individualized treatment strategies for recurrent EC.

**Keywords:** Endometrial cancer, recurrent disease, contrast-enhanced magnetic resonance imaging, computed tomography, treatment response, diagnostic accuracy

## Introduction

Endometrial cancer (EC) is among the most prevalent gynecologic malignancies, with a rising global incidence, particularly in countries with aging populations and increasing obesity rates [1]. Although advances have been made in the diagnosis and initial treatment of primary EC, recurrent cases remain a major clinical challenge [2]. Recurrence is associated with poor prognosis and often requires more complex management strategies [3]. Accurate evaluation of treatment response in recurrent EC is essential for guiding therapy, improving outcomes, and optimizing healthcare resource utilization [4].

Imaging plays a crucial role in assessing recurrent disease, enabling evaluation of tumor burden, therapeutic response, and recurrence detection [5]. Contrast-enhanced magnetic resonance imaging (CE-MRI) and computed tomography (CT) are two widely used imaging modalities [6]. CE-MRI offers superior contrast resolution and multiplanar imaging, providing detailed visualization of tumor morphology, local invasion, and adjacent structure involvement [7]. Its high sensitivity to soft tissue contrast facilitates differentiation between residual or recurrent tumor and post-treatment changes such as fibrosis or [8].

In contrast, CT is valued for its rapid acquisition of high-resolution pelvic and abdominal images

## Imaging evaluation of recurrent endometrial cancer

[9]. It is particularly effective in identifying calcifications, lymph node involvement, and structural features of masses or nodules [10], making it a key tool for assessing tumor architecture and distant metastases [11].

Despite these advantages, debate persists regarding the relative effectiveness of CE-MRI and CT in evaluating treatment cancer [12]. While previous studies have explored each modality independently, comparative analyses remain limited [13]. This retrospective case-control study aims to directly compare the diagnostic performance of CE-MRI and CT in assessing treatment response in patients with recurrent EC.

### Materials and methods

#### *Study design*

This study included 217 patients with recurrent EC treated at Yantaishan Hospital between January 2020 and December 2023. Patient data were retrieved from the hospital's electronic medical record system. Based on histopathological confirmation and treatment response evaluated using the Response Evaluation Criteria in Solid Tumors (1.1) [14], patients were divided into two groups: a response group and a non-response group. The response group (n = 102) included patients who achieved either a partial or complete response to treatment, while the non-response group (n = 115) included those with stable or progressive disease.

An internal validation cohort consisting of 142 patients from the same institution was established using identical inclusion and grouping criteria. Among them, 63 patients were classified in the response group, and 79 in the non-response group. Additionally, an external validation cohort comprising 168 patients from another institution was included, following the same eligibility and classification criteria. This cohort included 77 patients in the response group and 91 in the non-response group.

#### *Eligibility and grouping criteria*

This retrospective study was approved by the Institutional Review Board and Ethics Committee of Yantaishan Hospital. Informed consent was waived, as only de-identified data were used, posing no risk to patient care. The

waiver was granted in accordance with ethical and regulatory standards for retrospective research.

Inclusion criteria were: (1) patients aged 18-75 years who met the diagnostic criteria outlined in the International Federation of Gynecology and Obstetrics (FIGO) 2023 Cancer Report: FIGO Staging of EC [15]; (2) patients with primary EC who achieved complete remission after initial systemic treatment, maintained for at least 3 months in those receiving radiotherapy, or at least 6 months in those who did not; (3) histopathological confirmation that the recurrent lesion was identical to the primary tumor, indicating first recurrence; (4) patients who underwent surgical resection following recurrence; and (5) availability of complete preoperative contrast-enhanced MRI (CE-MRI), CT imaging data, and full clinical and pathological records.

Exclusion criteria included: (1) patients who did not undergo surgical treatment for EC; (2) those with rare histological subtypes such as clear cell carcinoma or sarcomatoid carcinoma; (3) presence of other malignancies; (4) individuals with severe cardiopulmonary disease or renal insufficiency; (5) patients with a history of severe allergic reactions to contrast agents; (6) pregnancy or lactation; (7) presence of pacemakers or other implanted electronic devices; (8) ferromagnetic foreign bodies (e.g., shrapnel, certain tattoo pigments); and (9) individuals with severe anxiety or claustrophobia (**Figure 1**).

#### *CE-MRI data acquisition*

All patients underwent contrast-enhanced MRI (CE-MRI) approximately two weeks prior to surgery. Scans were performed using a 1.5 T MRI scanner (Achieva and Intera; Philips Medical Systems, Best, the Netherlands) equipped with a phased-array torso coil. To minimize motion artifacts, patients were instructed to fast for 4-6 hours and to empty their bladder before the procedure. Additionally, 30 minutes before scanning, 20 mg of scopolamine butylbromide (Buscopan; Boehringer Ingelheim Korea, Seoul, Korea) was administered intramuscularly to reduce bowel peristalsis.

A fat-saturated, T1-weighted, three-dimensional fast field echo sequence was used. For dy-

## Imaging evaluation of recurrent endometrial cancer

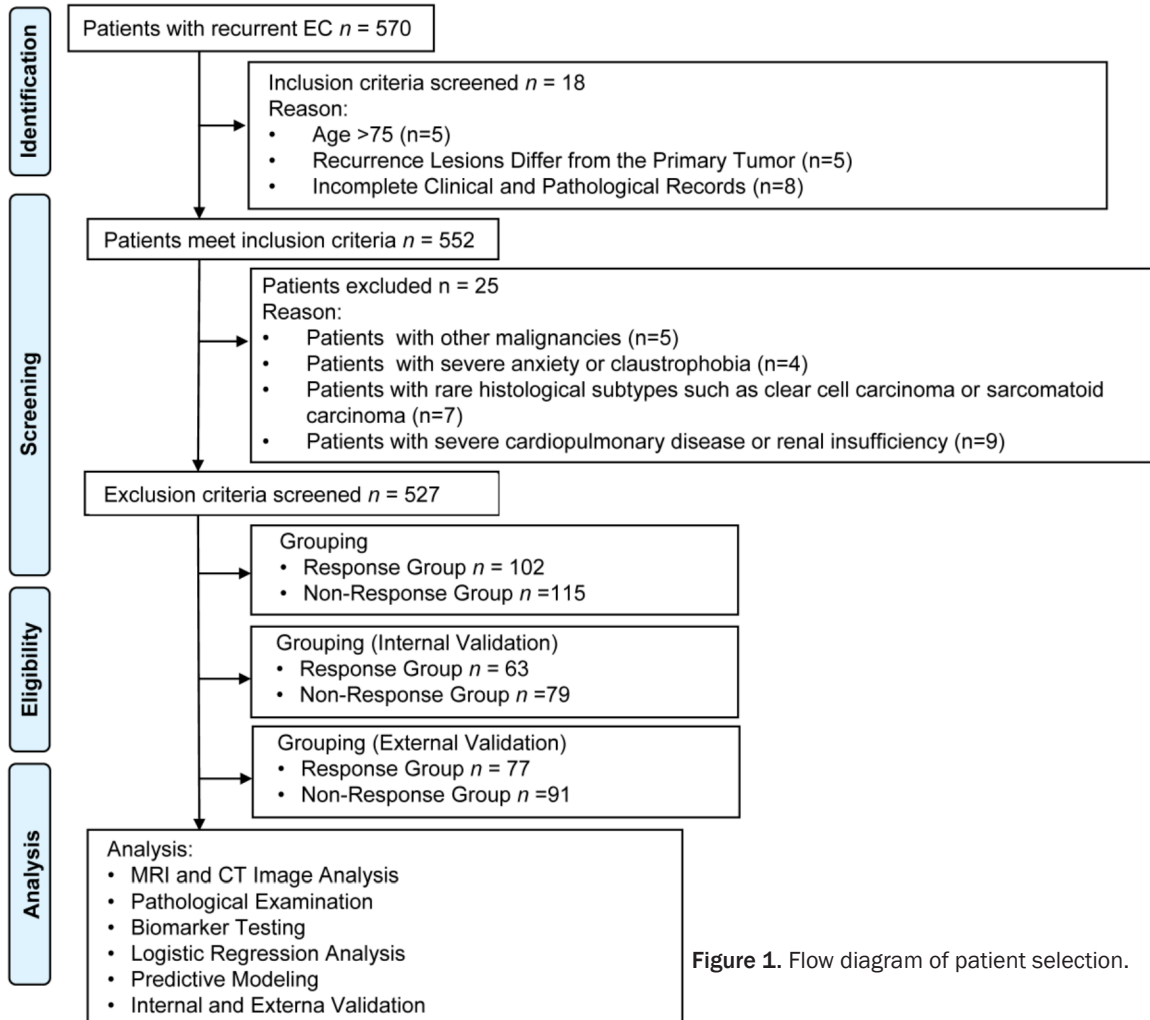


Figure 1. Flow diagram of patient selection.

dynamic CE-MRI, oblique axial images - perpendicular to the endometrial cavity - were obtained. The scan percentage was reduced to 60% to achieve a temporal resolution of 25-40 seconds, depending on uterine size. Loss in resolution was compensated by reconstructing the peripheral k-space from the final dynamic reference scan. Imaging commenced simultaneously with intravenous injection of gadolinium-based contrast (0.1 mmol/kg body weight) at 2 mL/s through an antecubital vein, acquiring 7-12 consecutive series over 4-6 minutes. The resulting coronal datasets were immediately reconstructed into sagittal, coronal, and oblique axial planes and transferred to the picture archiving and communication system (Marosis M-view, Infinitt, Seoul, Korea). For anatomical consistency, a slice thickness of 2 mm with no interslice gap was applied. The reconstruction process averaged one minute.

### Treatment modalities

Patients received various treatment regimens, including carboplatin plus paclitaxel, cisplatin plus doxorubicin, cisplatin plus paclitaxel, hormonal therapy, or other individualized therapies. These preoperative treatment strategies were considered potential confounders affecting treatment response and imaging features, and were thus summarized and analyzed in the baseline characteristics table.

### CE-MRI image analysis

All MRI data were anonymized by a physician not involved in image interpretation and uploaded to a dedicated study worklist on the PACS. Two genitourinary radiologists with 4 and 15 years of experience, respectively, along with a first-year resident, independently reviewed the CE-MRI scans in a randomized order. Reviewers

## Imaging evaluation of recurrent endometrial cancer

were informed of the study's objectives but were blinded to surgical and pathological outcomes. Their assessments, aided by T2-weighted imaging (T2WI) and diffusion-weighted imaging (DWI), included: presence of masses or nodules signal intensity on T1WI, T2WI, and DWI degree of contrast enhancement, invasion of adjacent structures, presence of ascites, hemorrhage, cystic changes, and calcification.

To evaluate consistency, inter-observer agreement was assessed using Cohen's kappa ( $\kappa$ ) for categorical variables and intraclass correlation coefficient (ICC) for continuous variables.  $\kappa$  values ranged from 0.78 to 0.89, indicating substantial to almost perfect agreement. ICC values ranged from 0.87 to 0.93, demonstrating excellent reliability. Discrepancies were resolved by a third senior radiologist (> 15 years experience), with consensus serving as the final determination. These measures ensured high reproducibility and reliability of imaging analysis, thereby strengthening the validity of study conclusions.

### *CT data acquisition*

All patients underwent CT scans approximately two weeks before surgery. Scans were performed during breath-hold at end-inspiration with patients in the supine position using a 256-slice CT scanner (Revolution CT; GE Healthcare, Waukesha, WI, USA). Scanning parameters were as follows: tube voltage 120-140 kV, tube current 250-300 mAs, slice thickness 0.625-1.25 mm, pitch 1.0-1.5, display field 350 mm, and matrix size 512 × 512.

During contrast-enhanced scanning, 60-100 mL of non-ionic iodinated contrast agent was rapidly injected into the antecubital vein. Contrast-enhanced phases were acquired at 25 and 60 seconds post-injection. The resulting image data were transmitted to the workstation for further processing, including multiplanar reconstruction, curved planar reformation, and other post-processing techniques.

### *CT image analysis*

Two experienced physicians independently evaluated the CT images using the 3D Slicer software. Tumor regions of interest were manually segmented layer by layer. The evaluated features included: maximum tumor diameter, le-

sion borders, shape, CT attenuation (density), lymph node involvement, presence of masses or nodules, contrast enhancement, and evidence of distant metastases. All evaluations were performed with the physicians blinded to clinical and pathological information.

### *Pathological examination*

After clinical diagnosis of recurrent EC, patients underwent biopsy via hysteroscopy. A physician visually examined the endometrium and obtained tissue samples using biopsy forceps. These samples were immediately sent to the pathology lab for processing. Two pathologists evaluated tumor histology, and discrepancies were resolved by discussion until consensus was reached.

Following surgery, resected tumor specimens were fixed in formalin, embedded in paraffin, and sectioned. Multiple sections were stained with hematoxylin and eosin and evaluated under light microscopy. Two experienced pathologists independently reviewed each slide, with any differences resolved through discussion.

Based on pathological and biopsy findings, disease progression and treatment response were evaluated according to the RECIST version 1.1 criteria, classifying patients as having complete response, partial response, stable disease, or progressive disease.

### *Biomarker testing*

Paraffin-embedded tissue sections were processed using an NS40 automatic immunohistochemical staining system (Dakewe Biotech Co., Ltd, Shenzhen, China). Estrogen receptors (ER) and progesterone receptors (PR) status were evaluated using a Nikon optical microscope (Nikon, Japan).

Serum levels of tumor markers - including cancer antigen 125 (CA125), cancer antigen 19-9 (CA19-9), carcinoembryonic antigen (CEA), and ovarian cancer-related protein 1 (OVX1) - were measured using the BK12200 chemiluminescence immunoassay analyzer (BIOBASE, Jinan, China).

### *Statistical analysis*

Statistical analysis was performed using SPSS software version 29.0 (SPSS Inc., Chicago, IL,

## Imaging evaluation of recurrent endometrial cancer

USA). Categorical variables were reported as frequencies and percentages [n (%)], and analyzed using the chi-square test, with the test statistic denoted as  $\chi^2$ . Continuous variables were tested for normal distribution using the Shapiro-Wilk method. Normally distributed continuous data were presented as mean  $\pm$  standard deviation ( $X \pm s$ ) and compared between groups using the t-test. A two-sided  $p$ -value  $< 0.05$  was considered statistically significant.

Receiver operating characteristic (ROC) curves were generated separately based on CE-MRI and CT imaging features to establish CE-MRI and CT diagnostic models. Additionally, imaging features from both modalities, along with the most discriminative biomarkers, were combined to construct a comprehensive diagnostic model.

The diagnostic performances of the three models were compared. Internal and external validation was conducted using independent cohorts of recurrent EC patients. Calibration curves were plotted to assess the agreement between predicted probabilities and observed outcomes, with ideal calibration indicated by a 45-degree line. Model calibration was further evaluated using the Hosmer-Lemeshow test, with  $P > 0.05$  indicating a good fit.

### Results

#### *Comparison of demographic and baseline characteristics*

A total of 217 patients were included, with 102 in the response group and 115 in the non-response group (**Table 1**). There were no significant differences between the two groups in terms of mean age, body mass index (BMI), marital status, education level, FIGO stage at initial diagnosis, histological subtype, and prior treatment (all  $P > 0.05$ ).

Preoperative treatment regimens were also similar between groups ( $P = 0.796$ ), with the most common regimen being carboplatin combined with paclitaxel. Additionally, no significant group differences were observed in symptoms such as vaginal discharge, lymphedema, gastrointestinal complaints, endocrine disorders, or urinary tract issues (all  $P > 0.05$ ).

These findings suggest that the two groups were well-matched in baseline characteristics,

supporting a valid comparison of CE-MRI and CT in evaluating treatment response.

#### *Comparison of biomarker profiles*

The ER positivity rate was similar between the groups, at 68.63% in the response group and 58.26% in the non-response group ( $P = 0.114$ ) (**Table 2**). Similarly, no significant differences were observed for PR positivity (77.45% vs. 82.61%,  $P = 0.341$ ), CA125 (69.61% vs. 59.13%,  $P = 0.108$ ), CA19-9 (50.98% vs. 46.09%,  $P = 0.472$ ), CEA (20.59% vs. 23.48%,  $P = 0.609$ ), and OVX1 (54.9% vs. 45.22%,  $P = 0.154$ ).

However, based on an updated analysis (**Table 3**), significant differences were observed in biomarker expression. The ER positivity rate was significantly lower in the response group (50.00%) compared to the non-response group (68.70%,  $P = 0.005$ ), as was the PR positivity rate (70.59% vs. 84.35%,  $P = 0.015$ ).

Positivity rates for CA125, CA19-9, and CEA were also significantly lower in the response group (48.04%, 33.33%, and 14.71%, respectively) than in the non-response group (62.61%, 48.70%, and 30.43%, with  $P$ -values of 0.031, 0.022, and 0.006, respectively). OVX1 positivity was 40.20% in the response group, significantly lower than 57.39% in the non-response group ( $P = 0.011$ ).

These results suggest that biomarker expression may influence treatment responsiveness and correlate with imaging findings.

#### *Comparison of CE-MRI imaging features*

The presence of masses or nodules was significantly lower in the response group (41.18%) compared to the non-response group (61.74%,  $P = 0.002$ ) (**Table 4**).

Regarding signal characteristics, the response group showed significantly lower frequencies of low signal intensity on T1WI ( $P = 0.002$ ), high signal intensity on T2WI ( $P = 0.006$ ), and high signal intensity on DWI.

Contrast enhancement patterns also differed significantly: dynamic enhancement and ring enhancement were less common in the response group (both  $P < 0.001$ ), as was delayed enhancement ( $P = 0.007$ ).

## Imaging evaluation of recurrent endometrial cancer

**Table 1.** Baseline characteristics

Parameters	Response Group (n = 102)	Non-Response Group (n = 115)	t/ $\chi^2$	P
Age (years)	56.75 ± 5.27	56.32 ± 5.34	0.597	0.551
BMI (kg/m)	20.27 ± 2.28	20.15 ± 2.81	0.349	0.728
Marital status (Married/Others)	91 (89.22%)/11 (10.78%)	97 (84.35%)/18 (15.65%)	1.106	0.293
Educational level			0.803	0.669
Junior high school and below	48 (47.06%)	55 (47.83%)		
high school and vocational school	35 (34.31%)	34 (29.57%)		
College and above	19 (18.63%)	26 (22.61%)		
FIGO stage at primary diagnosis			1.33	0.722
Stage I	39 (38.24%)	46 (40%)		
Stage II	9 (8.82%)	8 (6.96%)		
Stage III	36 (35.29%)	35 (30.43%)		
Stage IV	18 (17.65%)	26 (22.61%)		
Histologic subtype			2.633	0.756
Endometrioid carcinoma	66 (64.71%)	69 (60%)		
Serous	4 (3.92%)	8 (6.96%)		
Type II EC	13 (12.75%)	18 (15.65%)		
Mixed carcinoma	7 (6.86%)	10 (8.7%)		
Undifferentiated	4 (3.92%)	2 (1.74%)		
Others	8 (7.84%)	8 (6.96%)		
Previous therapy			1.255	0.534
Chemotherapy	38 (37.25%)	48 (41.74%)		
Radiotherapy	60 (58.82%)	65 (56.52%)		
Surgery	4 (3.92%)	2 (1.74%)		
Preoperative Treatment Plan			1.671	0.796
Carboplatin + Paclitaxel	39 (38.24%)	37 (32.17%)		
Cisplatin + Doxorubicin	21 (20.59%)	26 (22.61%)		
Cisplatin + Paclitaxel	25 (24.51%)	28 (24.35%)		
Hormone Therapy	9 (8.82%)	10 (8.7%)		
Others	8 (7.84%)	14 (12.17%)		
Vaginal discharge	21 (20.59%)	28 (24.35%)	0.437	0.509
Lymphedema	25 (24.51%)	33 (28.7%)	0.484	0.487
Gastrointestinal issues	13 (12.75%)	17 (14.78%)	0.188	0.664
Endocrine disorders	16 (15.69%)	21 (18.26%)	0.253	0.615
Urinary system problems	23 (22.55%)	28 (24.35%)	0.097	0.755

BMI: Body Mass Index; FIGO: International Federation of Gynecology and Obstetrics; EC: Endometrial Carcinoma; Gastrointestinal issues include constipation, diarrhea, and abdominal bloating; Urinary system problems include frequent urination, urgency, and dysuria.

Invasion of adjacent structures was more frequent in the non-response group. Bladder wall thickening was observed in 3.92% of the response group versus 14.78% in the non-response group ( $P = 0.007$ ), and rectal wall thickening in 4.90% vs. 15.65% ( $P = 0.01$ ). The incidence of ascites was also lower in the response group (2.94% vs. 15.65%,  $P = 0.002$ ).

No significant differences were observed in cystic changes ( $P = 0.05$ ), calcification ( $P =$

0.238), or pelvic wall soft tissue thickening ( $P = 0.102$ ).

### *Comparison of CT imaging features*

The mean longest diameter of lesions was significantly smaller in the response group (6.32 ± 3.36 mm) compared to the non-response group (9.82 ± 3.07 mm,  $P < 0.001$ ) (Table 5).

Lesions in the response group more frequently had clear margins (51.96% vs. 34.78%,  $P =$

## Imaging evaluation of recurrent endometrial cancer

**Table 2.** Comparison of baseline positive rates of biomarkers between the two groups

Variable	Response Group (n = 102)	Non-Response Group (n = 115)	$\chi^2$	P
ER	70 (68.63%)	67 (58.26%)	2.496	0.114
PR	79 (77.45%)	95 (82.61%)	0.905	0.341
CA125	71 (69.61%)	68 (59.13%)	2.577	0.108
CA19-9	52 (50.98%)	53 (46.09%)	0.518	0.472
CEA	21 (20.59%)	27 (23.48%)	0.262	0.609
OVX1	56 (54.9%)	52 (45.22%)	2.028	0.154

ER: Estrogen Receptor (Positive:  $\geq 1\%$  of Cells Expressing); PR: Progesterone Receptor (Positive:  $\geq 1\%$  of Cells Expressing); CA125: Cancer Antigen 125 (Positive:  $\geq 1\%$  of Cells Expressing); CA19-9: Cancer Antigen 19-9 (Positive Criterion:  $> 37.00$  U/mL); CEA: Carcinoembryonic Antigen (Positive Criterion:  $> 5.0$  ng/mL); OVX1: Ovarian Cancer-related Protein 1 (Positive Criterion:  $> 7.2$  U/mL).

**Table 3.** Comparison of positive rates of biomarkers between the two groups one week before surgery

Variable	Response Group (n = 102)	Non-Response Group (n = 115)	$\chi^2$	P
ER	51 (50%)	79 (68.7%)	7.866	0.005
PR	72 (70.59%)	97 (84.35%)	5.941	0.015
CA125	49 (48.04%)	72 (62.61%)	4.651	0.031
CA19-9	34 (33.33%)	56 (48.7%)	5.256	0.022
CEA	15 (14.71%)	35 (30.43%)	7.542	0.006
OVX1	41 (40.2%)	66 (57.39%)	6.394	0.011

**Table 4.** Comparison of CE-MRI imaging features between the two groups

Variable	Response Group (n = 102)	Non-Response Group (n = 115)	$\chi^2$	P
Mass or nodule	42 (41.18%)	71 (61.74%)	9.158	0.002
Signal intensity				
T1WI low signal intensity	36 (35.29%)	65 (56.52%)	9.79	0.002
T2WI high signal intensity	45 (44.12%)	72 (62.61%)	7.439	0.006
DWI high signal intensity	35 (34.31%)	74 (64.35%)	19.505	$< 0.001$
Contrast enhancement				
Dynamic enhancement	32 (31.37%)	72 (62.61%)	21.133	$< 0.001$
Delayed enhancement	46 (45.1%)	73 (63.48%)	7.374	0.007
Ring enhancement	19 (18.63%)	46 (40%)	11.768	$< 0.001$
Invasion of adjacent structures				
Bladder wall thickening	4 (3.92%)	17 (14.78%)	7.295	0.007
Rectal wall thickening	5 (4.9%)	18 (15.65%)	6.593	0.01
Pelvic wall soft tissue thickening	4 (3.92%)	11 (9.57%)	2.676	0.102
Ascites	3 (2.94%)	18 (15.65%)	9.992	0.002
Hemorrhage	5 (4.9%)	13 (11.3%)	2.913	0.088
Cystic change	6 (5.88%)	16 (13.91%)	3.827	0.05
Calcification	2 (1.96%)	7 (6.09%)	1.393	0.238

CE-MRI: Contrast-enhanced Magnetic Resonance Imaging; T1WI: T1-weighted imaging; T2WI: T2-weighted imaging; DWI: diffusion-weighted imaging.

0.011) and regular shapes (50.98% vs. 30.43%,  $P = 0.002$ ). The response group also exhibited higher average CT values ( $37.41 \pm 7.35$  HU vs.  $32.25 \pm 7.74$  HU,  $P < 0.001$ ).

Lymph node metastasis was less common in the response group (43.14% vs. 60.87%,  $P = 0.009$ ), as was the presence of masses or nodules (41.18% vs. 58.26%,  $P = 0.012$ ).

## Imaging evaluation of recurrent endometrial cancer

**Table 5.** Comparison of CT imaging features between the two groups

Variable	Response Group (n = 102)	Non-Response Group (n = 115)	$\chi^2$	P
Longest Diameter (mm)	6.32 ± 3.36	9.82 ± 3.07	8.038	< 0.001
Borders (clear/blurry)	53 (51.96%)	40 (34.78%)	6.513	0.011
Shape (regular/irregular)	52 (50.98%)	35 (30.43%)	9.5	0.002
CT value (HU)	37.41 ± 7.35	32.25 ± 7.74	5.024	< 0.001
Lymph node metastasis	44 (43.14%)	70 (60.87%)	6.816	0.009
Mass or nodule	42 (41.18%)	67 (58.26%)	6.311	0.012
Early enhancement	51 (50%)	78 (67.83%)	7.125	0.008
Delayed enhancement	44 (43.14%)	71 (61.74%)	7.509	0.006
Ring enhancement	29 (28.43%)	35 (30.43%)	0.104	0.747
Distant metastasis	4 (3.92%)	7 (6.09%)	0.527	0.468

CT: Computed Tomography; CT value: Computed Tomography number.

**Table 6.** Multivariate logistic regression analysis of CE-MRI imaging

Variable	SE	Wald	OR	95% CI	P
CE-MRI Mass or nodule	0.504	2.362	3.292	1.225-8.848	0.018
T1WI low signal intensity	0.503	1.245	1.871	0.698-5.017	0.033
T2WI high signal intensity	0.502	1.632	2.268	0.848-6.067	0.043
DWI high signal intensity	0.510	3.217	5.167	1.900-14.052	0.001
Dynamic enhancement	0.522	3.457	6.078	2.185-16.911	< 0.001
Delayed enhancement	0.485	0.924	1.566	0.605-4.053	0.035
CE-MRI Ring enhancement	0.530	1.376	2.074	0.734-5.861	0.029
CE-MRI Bladder wall thickening	0.986	1.984	7.071	1.024-48.823	0.047
CE-MRI Rectal wall thickening	0.891	2.357	8.176	1.425-46.909	0.018
CE-MRI Ascites	1.057	0.708	2.113	0.266-16.785	0.039

SE: Standard Error; Wald: Wald Test; OR: Odds Ratio; 95% CI: 95% Confidence Interval.

Early enhancement (50% vs. 67.83%,  $P = 0.008$ ) and delayed enhancement (43.14% vs. 61.74%,  $P = 0.006$ ) were also less frequent in the response group.

No significant differences were found in ring enhancement ( $P = 0.747$ ) or distant metastasis ( $P = 0.468$ ).

These findings underscore the relevance of CT imaging characteristics in evaluating treatment response in recurrent EC.

### Multivariate logistic regression analysis of CE-MRI imaging

Multivariate logistic regression identified several CE-MRI features significantly associated with treatment response in patients with recurrent EC. These included the presence of a mass or nodule, low signal intensity on T1WI, high signal intensity on T2WI, high signal intensity on

DWI, dynamic enhancement, delayed enhancement, ring enhancement, bladder wall thickening, rectal wall thickening, and ascites, all showing positive associations with treatment response ( $OR > 1$ ) (**Table 6**).

### ROC curve of CE-MRI imaging

ROC curve analysis of CE-MRI features demonstrated that dynamic enhancement [area under the curve (AUC) = 0.656] and high signal intensity on DWI (AUC = 0.650) showed relatively strong diagnostic value for evaluating treatment response in recurrent EC (**Table 7**). Other features, including presence of a mass or nodule (AUC = 0.603), low signal intensity on T1WI (AUC = 0.606), and ring enhancement (AUC = 0.607), showed moderate diagnostic performance.

Although bladder and rectal wall thickening and ascites exhibited high specificity, their low sen-

## Imaging evaluation of recurrent endometrial cancer

**Table 7.** ROC analysis for CE-MRI imaging

Variable	Best threshold	Sensitivities	Specificities	AUC	Youden index
CE-MRI Mass or nodule	0.500	0.617	0.588	0.603	0.205
T1WI low signal intensity	0.500	0.565	0.647	0.606	0.212
T2WI high signal intensity	0.500	0.626	0.559	0.592	0.185
DWI high signal intensity	0.500	0.643	0.657	0.650	0.300
Dynamic enhancement	0.500	0.626	0.686	0.656	0.312
Delayed enhancement	0.500	0.635	0.549	0.592	0.184
CE-MRI Ring enhancement	0.500	0.400	0.814	0.607	0.214
CE-MRI Bladder wall thickening	0.500	0.148	0.961	0.554	0.109
CE-MRI Rectal wall thickening	0.500	0.157	0.951	0.554	0.108
CE-MRI Ascites	0.500	0.157	0.971	0.564	0.128

ROC: Receiver Operating Characteristic curve; AUC: Area Under the Curve.

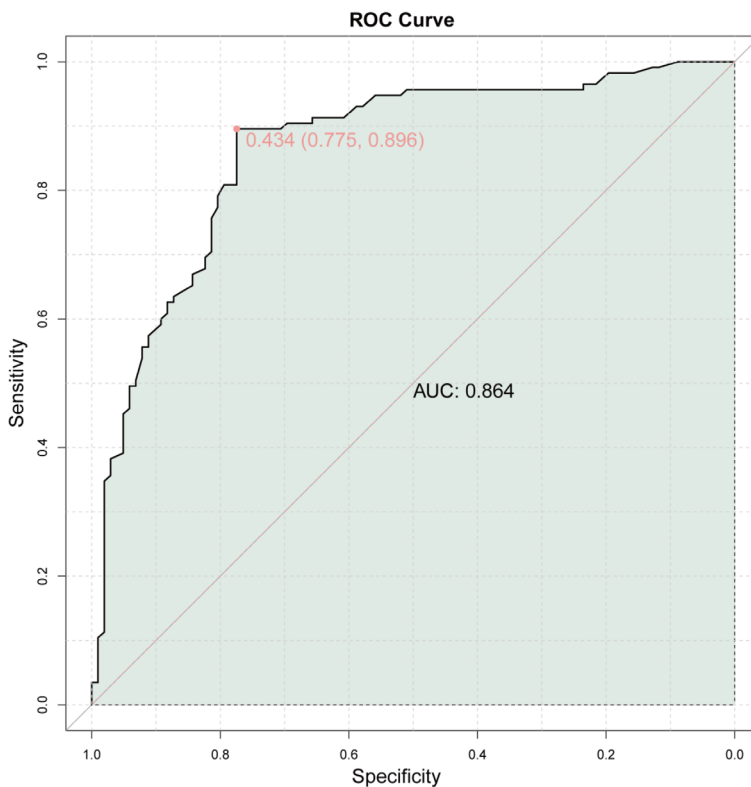


**Figure 2.** ROC Curve of CE-MRI imaging. ROC: Receiver Operating Characteristic curve; AUC: Area Under the Curve; CE-MRI: contrast-enhanced magnetic resonance imaging.

sensitivity limited their overall diagnostic utility. These findings suggest that dynamic enhancement and DWI hyperintensity may serve as more reliable imaging indicators of treatment response.

An integrated predictive model incorporating multiple CE-MRI features demonstrated excellent predictive performance, with an AUC of

0.864 (**Figure 2**), highlighting its utility in predicting treatment outcomes for recurrent EC.

### *Multivariate logistic regression analysis of CT imaging*

Multivariate logistic regression analysis of CT imaging features identified several parameters significantly associated with treatment response in recurrent EC (**Table 8**). These included a larger longest lesion diameter, indistinct lesion margins, irregular shape, lower CT attenuation values, presence of lymph node metastasis, presence of a mass or nodule, early enhancement, and delayed enhancement.

Among these, the longest lesion diameter had the strongest association with treatment response, with an odds ratio of 7.220. These results indicate that CT imaging pro-

vides valuable predictive information for assessing treatment response.

### *ROC curve of CT imaging*

ROC analysis revealed varying diagnostic performance of CT imaging features in evaluating treatment response. Among all parameters, lesion margin clarity demonstrated the highest

## Imaging evaluation of recurrent endometrial cancer

**Table 8.** Multivariate logistic regression analysis of CT imaging

Variable	SE	Wald	OR	95% CI	P
Longest Diameter (mm)	0.505	3.911	7.220	2.681-19.446	< 0.001
Borders (clear/blurry)	0.541	-1.352	0.481	0.167-1.390	0.037
Shape (regular/irregular)	0.515	-0.705	0.696	0.254-1.908	0.041
CT value (HU)	0.524	-2.736	0.239	0.086-0.666	0.006
CT Lymph node metastasis	0.500	2.114	2.875	1.080-7.655	0.035
CT Mass or nodule	0.494	0.111	1.056	0.401-2.780	0.031
CT Early enhancement	0.509	0.651	1.393	0.514-3.776	0.045
CT Delayed enhancement	0.484	1.554	2.121	0.822-5.475	0.032

**Table 9.** ROC analysis for CT imaging

Variable	Best threshold	Sensitivities	Specificities	AUC	Youden index
Longest Diameter (mm)	0.500	0.652	0.520	0.586	0.172
Borders (clear/blurry)	7.590	0.800	0.676	0.781	0.476
Shape (regular/irregular)	0.500	0.696	0.510	0.603	0.206
CT value (HU)	31.615	0.470	0.804	0.680	0.274
CT Lymph node metastasis	0.500	0.609	0.569	0.589	0.178
CT Mass or nodule	0.500	0.583	0.588	0.585	0.171
CT Early enhancement	0.500	0.678	0.500	0.589	0.178
CT Delayed enhancement	0.500	0.617	0.569	0.593	0.186

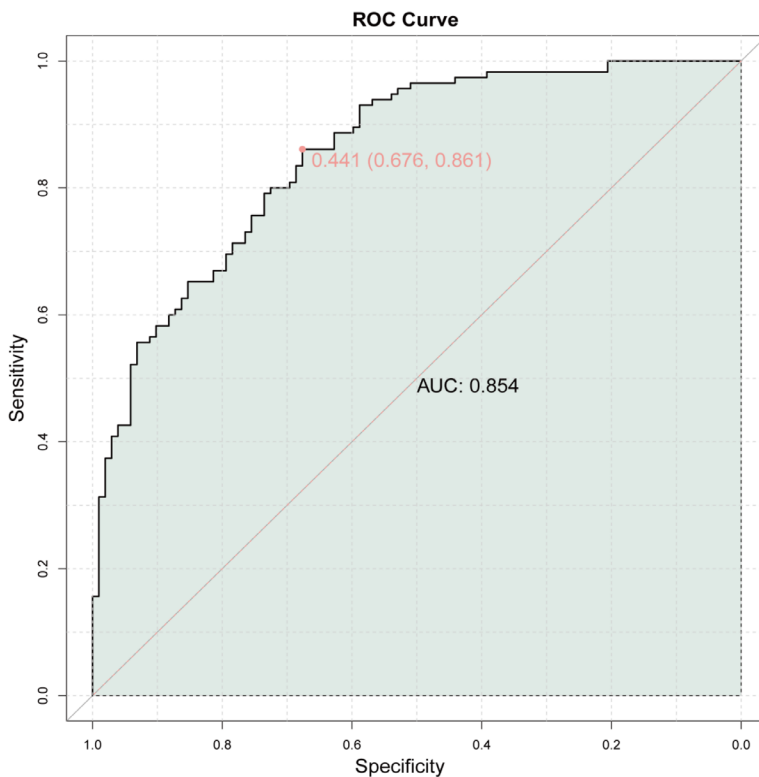


**Figure 3.** ROC Curve of CT imaging. CT: computed tomography.

diagnostic accuracy, with a sensitivity of 0.800, specificity of 0.676, AUC of 0.781, and a Youden

index of 0.476, making it the most effective single indicator (**Table 9**).

Lesion longest diameter (AUC = 0.586) and shape (AUC = 0.603) showed moderate diagnostic performance, whereas CT attenuation values exhibited high specificity (0.804) but lower sensitivity (0.470), with an AUC of 0.680 - indicating that higher CT values may suggest a better response to treatment.

Other features, including lymph node metastasis, masses or nodules, and early enhancement, had limited diagnostic utility (AUCs ranging from 0.585 to 0.593). Delayed enhancement also showed moderate performance with an AUC of 0.593.

A combined CT-based predictive model achieved a high diagnostic value, with an AUC of 0.854 (**Figure 3**), supporting its efficacy in predicting therapeutic outcomes.

## Imaging evaluation of recurrent endometrial cancer

**Table 10.** Multivariate logistic regression analysis of integrated model

Variable	SE	Wald	OR	95% CI	P
One week before surgery ER	0.505	1.632	2.280	0.848-6.132	0.033
One week before surgery CEA	0.607	1.559	2.577	0.784-8.469	0.039
One week before surgery OVX1	0.494	0.875	1.540	0.585-4.052	0.042
DWI high signal intensity	0.510	3.217	5.167	1.900-14.052	0.001
Dynamic enhancement	0.522	3.457	6.078	2.185-16.911	< 0.001
CE-MRI Ring enhancement	0.530	1.376	2.074	0.734-5.861	0.039
Longest Diameter (mm)	0.505	3.911	7.220	2.681-19.446	< 0.001
Shape (regular/irregular)	0.515	-0.705	0.696	0.254-1.908	0.041
CT value (HU)	0.524	-2.736	0.239	0.086-0.666	0.006

**Table 11.** ROC analysis for integrated model

Variable	Best threshold	Sensitivities	Specificities	AUC	Youden index
One week before surgery ER	0.500	0.687	0.500	0.593	0.187
One week before surgery CEA	0.500	0.304	0.853	0.579	0.157
One week before surgery OVX1	0.500	0.574	0.598	0.586	0.172
DWI high signal intensity	0.500	0.643	0.657	0.650	0.300
Dynamic enhancement	0.500	0.626	0.686	0.656	0.312
CE-MRI Ring enhancement	0.500	0.400	0.814	0.607	0.214
Longest Diameter (mm)	7.670	0.783	0.667	0.773	0.450
Shape (regular/irregular)	0.500	0.696	0.510	0.603	0.206
CT value (HU)	32.250	0.548	0.814	0.695	0.362

### *Multivariate logistic regression analysis of integrated model*

Multivariate logistic regression of the integrated model, which combined imaging and biomarker indicators, identified several significant predictors of treatment response in recurrent EC (**Table 10**).

Notably, higher preoperative levels of ER, CEA, and OVX1, as well as high signal intensity on DWI, dynamic enhancement, longer lesion diameter, and ring enhancement on CE-MRI were all positively associated with treatment response (OR > 1). In contrast, irregular lesion shape and lower CT attenuation were negatively associated with treatment response (OR < 1).

Among these, dynamic enhancement (OR = 6.078) and lesion diameter (OR = 7.220) had the strongest predictive value. These findings demonstrate that an integrated model combining imaging and biomarker features provides robust prediction of treatment efficacy in recurrent EC.

### *ROC curve analysis of the integrated model*

ROC analysis of the integrated model revealed that the longest lesion diameter had the highest diagnostic performance, with an AUC of 0.773 and the largest Youden index (0.450), indicating it was the most discriminatory feature for predicting treatment response (**Table 11**). Dynamic enhancement and CT attenuation values also demonstrated moderate to good discriminatory power, with AUCs of 0.656 and 0.695, and Youden indices of 0.312 and 0.362, respectively.

In contrast, preoperative CEA levels had the lowest diagnostic value (AUC = 0.579; Youden index = 0.157), indicating limited predictive utility. Other features, including ER, OVX1, high DWI signal intensity, CE-MRI ring enhancement, and lesion shape (regular vs. irregular), showed moderate discrimination but were less robust than the longest diameter or CT values.

These results suggest that the integrated model - particularly when incorporating the longest lesion diameter and CT value - can provide

## Imaging evaluation of recurrent endometrial cancer

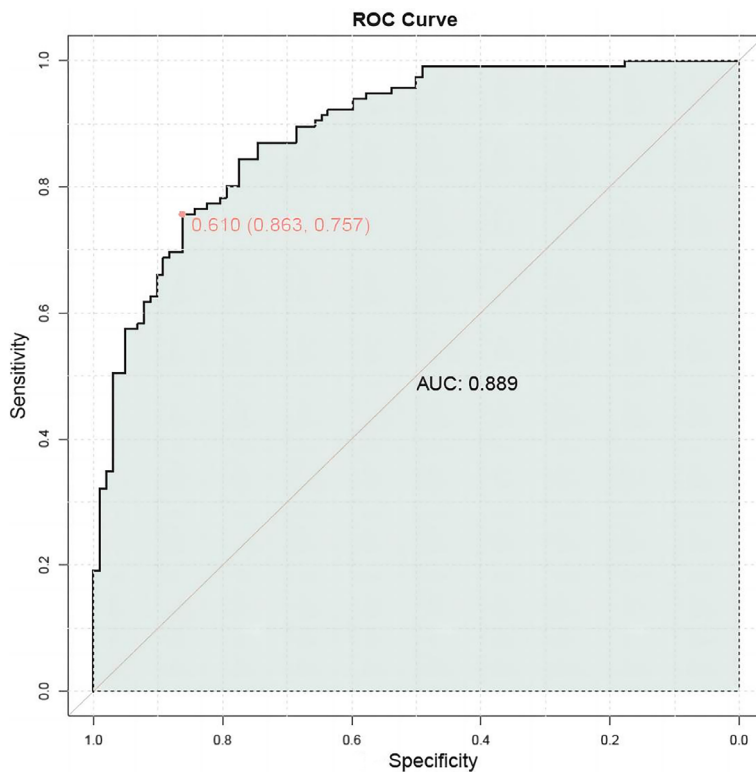


**Figure 4.** ROC Curve of the Integrated model.

clinically useful information for predicting treatment response in recurrent EC. The combination of these features may aid clinicians in identifying patients more likely to respond to treatment, thereby facilitating individualized therapeutic strategies.

By integrating CE-MRI, CT, and preoperative biomarker data, we constructed a comprehensive predictive model for treatment response in recurrent EC. This model achieved a high diagnostic performance, with an AUC of 0.889 (**Figure 4**), indicating excellent discriminatory capacity.

### *Diagnostic performance*

CE-MRI alone yielded an AUC of 0.864, with an accuracy of 82.4%, sensitivity of 78.3%, and specificity of 86.3% (**Table 12**). The positive predictive value (PPV) was 47.5%, and the negative predictive value (NPV) was 92.1%.

CT imaging demonstrated a slightly lower AUC of 0.854, with accuracy at 81.5%, sensitivity at 81.2%, and specificity at 83.4%. PPV and NPV were 36.2% and 92.7%, respectively.

The integrated model showed superior diagnostic performance, achieving an AUC of 0.889 and an accuracy of 86.7%. Notably, it significantly improved sensitivity to 94.3% while maintaining specificity at 81.2%. The PPV and NPV were 52.2% and 93.4%, respectively.

These findings suggest that although CE-MRI and CT are independently valuable, their combination with preoperative biomarkers in the integrated model enhances diagnostic accuracy, particularly improving sensitivity and overall predictive efficiency.

### *Calibration curve of the integrated model*

The calibration curve of the integrated model demonstrated excellent agreement between predicted and observed probabilities (**Figure 5**). The mean absolute error (MAE) was 0.021, indicating minimal deviation and strong calibration. Bootstrap resampling ( $n = 1,000$ ) further validated model robustness, with the bias-corrected curve closely following the ideal 45-degree line.

### *Demographic characteristics of the internal validation cohort*

Comparative analysis between the response group ( $n = 63$ ) and the non-response group ( $n = 79$ ) revealed no statistically significant differences in demographic or baseline clinical variables, including age, BMI, marital status, education level, FIGO stage at initial diagnosis, histological subtype, prior treatment modalities, preoperative treatment plans, or symptom profiles (e.g., vaginal discharge, lymphedema, gastrointestinal symptoms, endocrine disorders, urinary symptoms) ( $P > 0.05$ ) (**Table 13**).

### *Differential distribution of imaging and biomarker characteristics*

CEA positivity one week before surgery was significantly lower in the response group com-

## Imaging evaluation of recurrent endometrial cancer

**Table 12.** Diagnostic performance

Variable	AUC	Accuracy	Sensitivity	Specificity	PPV	NPV
CE-MRI	0.864	0.824	0.783	0.863	0.475	0.921
CT	0.854	0.815	0.812	0.834	0.362	0.927
Integrated model	0.889	0.867	0.943	0.812	0.522	0.934

PPV: positive predictive value; NPV: negative predictive value.

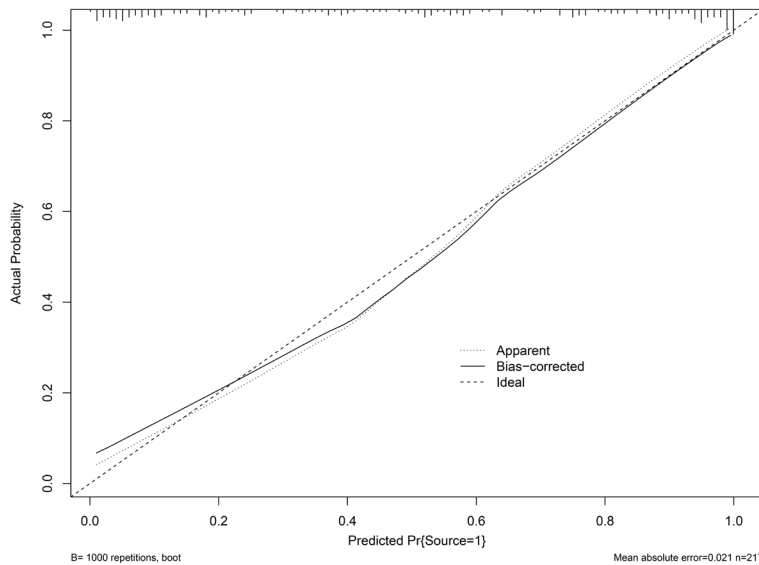


**Figure 5.** Calibration plot of the integrated model. B: Number of Bootstrap Replications.

pared to the non-response group ( $\chi^2 = 10.487$ ,  $P = 0.001$ ). OVX1 positivity also showed a similar trend ( $\chi^2 = 8.979$ ,  $P = 0.003$ ) (Table 14).

High signal intensity on DWI was less common in the response group ( $\chi^2 = 9.362$ ,  $P = 0.002$ ), as was the presence of dynamic enhancement ( $\chi^2 = 12.451$ ,  $P < 0.001$ ). The mean longest diameter was significantly smaller in the response group ( $t = 6.295$ ,  $P < 0.001$ ). Lesions with regular shape were more prevalent in the response group, while irregular shapes were more frequent in the non-response group ( $\chi^2 = 8.691$ ,  $P = 0.003$ ).

These findings suggest that patients with lower CEA and OVX1 positivity, absence of DWI hyperintensity and dynamic enhancement, smaller tumors, and regular lesion morphology are more likely to respond to treatment. These factors may serve as potential imaging and biomarker predictors to support personalized treatment planning.

### *Multivariate logistic regression analysis of the internal validation cohort*

Multivariate logistic regression analysis in the internal validation cohort identified several imaging and biomarker features significantly associated with treatment response in patients with recurrent EC (Table 15). Higher levels of CEA and OVX1 one week before surgery, high signal intensity on DWI, dynamic enhancement, and larger lesion diameter were all positively associated with treatment response. In contrast, irregular lesion shape was negatively associated with response. Among all variables, the longest diameter showed the strongest association, with an OR of 6.257. These findings confirm the initial analysis and support the predictive value of the integrated model that combines imaging and biomarker features.

greatest diameter showed the strongest association, with an OR of 6.257. These findings confirm the initial analysis and support the predictive value of the integrated model that combines imaging and biomarker features.

### *ROC curve of the internal validation cohort*

The ROC curve for the internal validation cohort showed excellent predictive performance, with an AUC of 0.889 (Figure 6), indicating strong discriminatory ability for predicting treatment response in patients with recurrent EC. This high AUC suggests the model is a reliable tool for supporting clinical decisions and personalized treatment planning.

### *Demographic characteristics of the external validation cohort*

In the external validation cohort, demographic and clinical characteristics were compared between the Response Group ( $n = 77$ ) and

## Imaging evaluation of recurrent endometrial cancer

**Table 13.** Demographic characteristics of the internal validation cohort

Parameters	Response Group (n = 63)	Non-Response Group (n = 79)	t/ $\chi^2$	P
Age (years)	55.26 ± 4.29	55.13 ± 4.38	0.178	0.859
BMI (kg/m)	20.63 ± 2.38	20.59 ± 2.46	0.083	0.934
Marital status (Married/Others)	54 (85.71%)/9 (14.29%)	64 (81.01%)/15 (18.99%)	0.552	0.458
Educational level			0.026	0.987
Junior high school and below	28 (44.44%)	36 (45.57%)		
high school and vocational school	20 (31.75%)	25 (31.65%)		
College and above	15 (23.81%)	18 (22.78%)		
FIGO stage at primary diagnosis			0.861	0.835
Stage I	25 (39.68%)	29 (36.71%)		
Stage II	6 (9.52%)	7 (8.86%)		
Stage III	23 (36.51%)	27 (34.18%)		
Stage IV	9 (14.29%)	16 (20.25%)		
Histologic subtype			1.680	0.891
Endometrioid carcinoma	39 (61.9%)	49 (62.03%)		
Serous	3 (4.76%)	6 (7.59%)		
Type II EC	6 (9.52%)	10 (12.66%)		
Mixed carcinoma	5 (7.94%)	6 (7.59%)		
Undifferentiated	4 (6.35%)	3 (3.8%)		
Others	6 (9.52%)	5 (6.33%)		
Previous therapy			0.066	0.968
Chemotherapy	25 (39.68%)	33 (41.77%)		
Radiotherapy	34 (53.97%)	41 (51.9%)		
Surgery	4 (6.35%)	5 (6.33%)		
Preoperative Treatment Plan			1.284	0.864
Carboplatin + Paclitaxel	25 (39.68%)	25 (31.65%)		
Cisplatin + Doxorubicin	11 (17.46%)	15 (18.99%)		
Cisplatin + Paclitaxel	13 (20.63%)	17 (21.52%)		
Hormone Therapy	6 (9.52%)	8 (10.13%)		
Others	8 (12.7%)	14 (17.72%)		
Vaginal discharge	14 (22.22%)	20 (25.32%)	0.184	0.668
Lymphedema	13 (20.63%)	23 (29.11%)	1.331	0.249
Gastrointestinal issues	9 (14.29%)	12 (15.19%)	0.023	0.880
Endocrine disorders	10 (15.87%)	15 (18.99%)	0.234	0.628
Urinary system problems	12 (19.05%)	19 (24.05%)	0.514	0.473

Non-Response Group (n = 91) (**Table 16**). No statistically significant differences were observed in age, BMI, marital status, education level, FIGO stage at initial diagnosis, histological subtype, prior treatments, preoperative treatment plan, or clinical symptoms (including vaginal discharge, lymphedema, gastrointestinal disorders, endocrine issues, or urinary symptoms).

### *Distribution of imaging and biomarker characteristics in the external validation cohort*

Significant differences were observed in several pre-surgical biomarkers and imaging fea-

tures between the Response and Non-Response groups (**Table 17**).

ER positivity one week before surgery was significantly lower in the Response Group (40.26%) than in the Non-Response Group (71.43%) ( $\chi^2 = 16.545$ ,  $P < 0.001$ ).

CEA positivity was also less frequent in the Response Group (12.99%) compared to the Non-Response Group (39.56%) ( $\chi^2 = 14.812$ ,  $P < 0.001$ ).

OVX1 positivity was significantly lower in the Response Group (35.06%) than in the Non-

## Imaging evaluation of recurrent endometrial cancer

**Table 14.** Characteristics of the data from the internal validation cohort

Variable	Response Group (n = 63)	Non-Response Group (n = 79)	t/ $\chi^2$	P
One week before surgery CEA	8 (12.70%)	29 (36.71%)	10.487	0.001
One week before surgery OVX1	20 (31.75%)	45 (56.96%)	8.979	0.003
DWI high signal intensity	22 (34.92%)	48 (60.76%)	9.362	0.002
Dynamic enhancement	18 (28.57%)	46 (58.23%)	12.451	< 0.001
Longest Diameter (mm)	6.38 ± 3.19	9.75 ± 3.16	6.295	< 0.001
Shape (regular/irregular)	31 (49.21%)	20 (25.32%)	8.691	0.003

**Table 15.** Multivariate logistic regression analysis of the internal validation cohort

Variable	SE	Wald	OR	95% CI	P
One week before surgery CEA	0.535	2.537	3.884	1.362-11.076	0.011
One week before surgery OVX1	0.440	2.438	2.922	1.234-6.919	0.015
DWI high signal intensity	0.442	2.873	3.561	1.497-8.469	0.004
Dynamic enhancement	0.451	3.487	4.814	1.990-11.644	< 0.001
Longest Diameter (mm)	0.450	4.078	6.257	2.592-15.106	< 0.001
Shape (regular/irregular)	0.464	-1.189	0.576	0.232-1.430	0.035

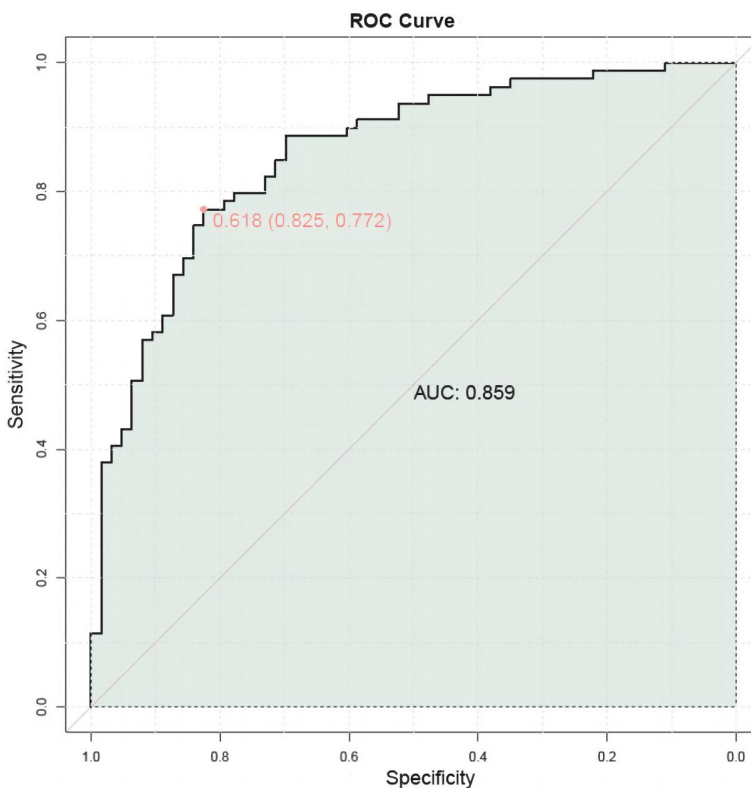


**Figure 6.** ROC curve of the internal validation integrated model.

Response Group (58.24%) ( $\chi^2 = 8.982$ ,  $P = 0.003$ ).

High signal intensity on DWI was more common in the Non-Response Group (61.54%) than in the Response Group (29.87%) ( $\chi^2 = 16.791$ ,  $P < 0.001$ ).

Dynamic enhancement was also more prevalent in the Non-Response Group (59.34%) than in the Response Group (32.47%) ( $\chi^2 = 12.091$ ,  $P < 0.001$ ).

The proportion of patients with longest diameter above threshold was higher in the Non-Response Group (42.86%) versus the Response Group (20.78%) ( $\chi^2 = 9.232$ ,  $P = 0.002$ ).

Irregular tumor shape was significantly more frequent in the Non-Response Group, with a mean value of  $9.48 \pm 3.55$  mm compared to  $6.41 \pm 3.63$  mm in the Response Group ( $\chi^2 = 5.543$ ,  $P < 0.001$ ).

These results suggest that lower ER, CEA, and OVX1 positivity, smaller tumor size, regular shape, and absence of DWI hyperintensity or dynamic enhancement indicators of favorable treatment response.

### ROC curve of the external validation cohort

The ROC curve for the external validation cohort, incorporating multiple imaging and bio-

## Imaging evaluation of recurrent endometrial cancer

**Table 16.** Demographic characteristics of the external validation cohort

Parameters	Response Group (n = 77)	Non-Response Group (n = 91)	t/ $\chi^2$	P
Age (years)	53.23 ± 5.3	53.52 ± 5.09	0.364	0.716
BMI (kg/m)	20.56 ± 3.06	20.69 ± 3.12	0.254	0.8
Marital status (Married/Others)	70 (90.91%)/7 (9.09%)	81 (89.01%)/10 (10.99%)	0.165	0.684
Educational level			0.029	0.986
Junior high school and below	34 (44.16%)	39 (42.86%)		
high school and vocational school	24 (31.17%)	29 (31.87%)		
College and above	19 (24.68%)	23 (25.27%)		
FIGO stage at primary diagnosis			0.722	0.868
Stage I	30 (38.96%)	38 (41.76%)		
Stage II	7 (9.09%)	7 (7.69%)		
Stage III	29 (37.66%)	30 (32.97%)		
Stage IV	11 (14.29%)	16 (17.58%)		
Histologic subtype			1.778	0.879
Endometrioid carcinoma	47 (61.04%)	53 (58.24%)		
Serous	4 (5.19%)	6 (6.59%)		
Type II EC	8 (10.39%)	14 (15.38%)		
Mixed carcinoma	7 (9.09%)	9 (9.89%)		
Undifferentiated	3 (3.9%)	3 (3.3%)		
Others	8 (10.39%)	6 (6.59%)		
Previous therapy			0.68	0.712
Chemotherapy	29 (37.66%)	39 (42.86%)		
Radiotherapy	42 (54.55%)	47 (51.65%)		
Surgery	6 (7.79%)	5 (5.49%)		
Preoperative Treatment Plan			1.975	0.74
Carboplatin + Paclitaxel	27 (35.06%)	27 (29.67%)		
Cisplatin + Doxorubicin	17 (22.08%)	21 (23.08%)		
Cisplatin + Paclitaxel	15 (19.48%)	23 (25.27%)		
Hormone Therapy	10 (12.99%)	8 (8.79%)		
Others	8 (10.39%)	12 (13.19%)		
Vaginal discharge	17 (22.08%)	22 (24.18%)	0.103	0.748
Lymphedema	16 (20.78%)	27 (29.67%)	1.731	0.188
Gastrointestinal issues	11 (14.29%)	14 (15.38%)	0.04	0.842
Endocrine disorders	13 (16.88%)	18 (19.78%)	0.233	0.63
Urinary system problems	18 (23.38%)	23 (25.27%)	0.081	0.775

marker variables, demonstrated outstanding predictive performance. The AUC of the integrated model was 0.918 (**Figure 7**), indicating excellent accuracy in predicting treatment response in patients with recurrent EC.

### Discussion

This retrospective case-control study compared the effects of CE-MRI and CT in evaluating treatment response for recurrent EC. We observed notable differences in the diagnostic performance of these imaging modalities. The

primary distinction between CE-MRI and CT lies in their respective imaging capabilities and sensitivities to various tissue characteristics [16]. CE-MRI provides detailed soft tissue contrast through T1-weighted, T2-weighted, and DWI imaging, offering comprehensive insights into the morphological and functional aspects of recurrent EC [17]. The high sensitivity of CE-MRI in detecting changes in tissue perfusion and cellularity explains its superior ability to differentiate treatment response levels, as indicated by its higher AUC and specificity compared to CT.

## Imaging evaluation of recurrent endometrial cancer

**Table 17.** Characteristics of the data of the external validation cohort

Variable	Response Group (n = 77)	Non-Response Group (n = 91)	t/ $\chi^2$	P
One week before surgery ER	31 (40.26%)	65 (71.43%)	16.545	< 0.001
One week before surgery CEA	10 (12.99%)	36 (39.56%)	14.812	< 0.001
One week before surgery OVX1	27 (35.06%)	53 (58.24%)	8.982	0.003
DWI high signal intensity	23 (29.87%)	56 (61.54%)	16.791	< 0.001
Dynamic enhancement	25 (32.47%)	54 (59.34%)	12.091	< 0.001
Longest Diameter (mm)	16 (20.78%)	39 (42.86%)	9.232	0.002
Shape (regular/irregular)	6.41 $\pm$ 3.63	9.48 $\pm$ 3.55	5.543	< 0.001

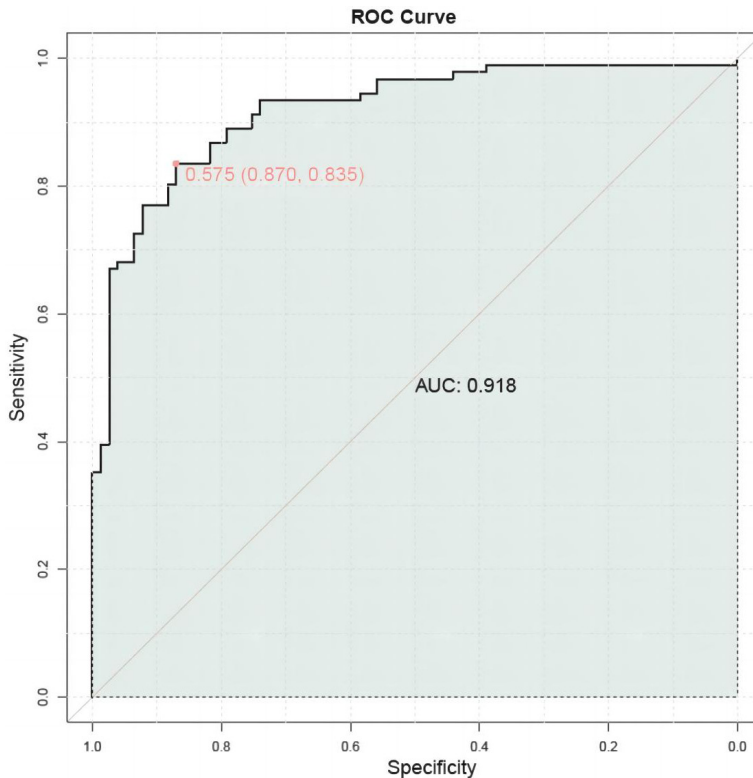


**Figure 7.** ROC curve of the external validation integrated model.

A key finding of this study is the superior diagnostic performance of the integrated model, which combines both CE-MRI and CT data. While individual imaging modalities provide valuable information, combining them with biomarker data offers a more comprehensive understanding of treatment response. This improvement is largely due to the complementary strengths of CE-MRI and CT. Mechanistically, the enhanced contrast resolution of CE-MRI increases its ability to detect subtle morphological changes in tumors and surrounding structural invasions, which are critical for monitoring disease progression and response [18, 19]. The superior performance of dynamic and

delayed enhancement features in MRI can be attributed to its proficiency in capturing the vascular and interstitial diffusion properties of tumors, which are often altered after therapeutic interventions [20]. These features make CE-MRI particularly effective in identifying residual or recurrent disease and differentiating it from treatment-related changes like fibrosis or necrosis [21].

In contrast, CT offers advantages in assessing calcifications, nodal involvement, and osseous structures, providing complementary benefits to CE-MRI [22]. Although CT exhibited slightly lower sensitivity and specificity compared to MRI, its ability to delineate the architecture of masses and nodules contributes to its utility in evaluating treatment response [23]. The diagnostic

value of features such as lesion borders and CT values underscores the importance of CT in assessing the structural aspects and geometric configurations of tumors, which may reflect the therapeutic impact [24].

A critical observation in our study was the complementary nature of CE-MRI and CT. While each modality provides substantial diagnostic information on its own, their combination enhances overall diagnostic efficacy, particularly in terms of sensitivity and predictive accuracy. This synergistic effect can be largely attributed to the integration of high-resolution soft tissue contrast from MRI and detailed

structural assessment from CT [25, 26]. Together, they allow for a comprehensive evaluation of tumor response, leading to more accurate predictions of therapeutic outcomes and potentially informing clinical decision-making [27].

To contextualize our findings, we reviewed several relevant studies. Sala et al. highlighted the significant role of dynamic contrast-enhanced MRI (DCE-MRI) in staging and assessing treatment response in EC, which aligns with our results for recurrent EC [28]. Lee et al. conducted a meta-analysis that suggested MRI has slightly better sensitivity than PET/CT, although PET/CT marginally outperforms MRI in specificity [29]. Both modalities showed comparable diagnostic performance in predicting pathological response to neoadjuvant therapy in locally advanced rectal cancer patients. Lee et al.'s study emphasized the value of combining structural and metabolic information to improve diagnostic accuracy [29]. This conclusion mirrors our findings of improved diagnostic performance by integrating CE-MRI and CT. Additionally, Hoffman et al. analyzed the advantages and limitations of CT in lung cancer screening. Although focused on lung cancer, their insights are applicable to understanding the role of CT in EC [30].

The increased sensitivity observed with the combined use of CE-MRI and CT was particularly valuable in the context of recurrent EC, which is crucial [31]. The ability to accurately identify and quantify these changes can significantly influence subsequent treatment strategies and patient management, potentially improving clinical outcomes [32].

Several factors may contribute to the differences in imaging efficacy observed between patient groups. For example, variations in tumor biology - such as differences in vascularity, cellular density, and molecular characteristics - can influence the imaging properties of CE-MRI and CT [33]. Furthermore, patient-specific factors, including previous treatment regimens, histological subtypes, and the presence of comorbid conditions, may affect imaging outcomes [34]. A deeper understanding of these factors can further refine imaging protocols and interpretation strategies, optimizing their use in clinical practice.

The findings of this study have significant implications for clinical practice, especially in managing recurrent EC. The enhanced diagnostic capability of combined imaging techniques allows for more precise evaluations of therapeutic responses, facilitating adjustments in treatment plans. This integrated approach could also be applied to other cancers where treatment-induced changes are difficult to assess using a single imaging modality.

While our study provides valuable insights into the comparative performance of CE-MRI and CT, it is important to acknowledge its inherent limitations. The retrospective design and reliance on de-identified data may introduce selection bias and limit the generalizability of the results. Additionally, despite efforts to match baseline characteristics across patient groups, potential confounding variables could still influence the observed outcomes. Future prospective studies with larger, more diverse cohorts could offer more definitive conclusions and further clarify the role of combined imaging techniques in oncological evaluations.

### Conclusion

In summary, this study demonstrates that while both CE-MRI and CT provide valuable diagnostic information for evaluating treatment responses in recurrent EC, their combined use significantly enhances diagnostic accuracy and sensitivity. This integrated imaging approach has the potential to improve patient management by enabling more precise assessments of treatment efficacy and guiding subsequent therapeutic decisions. Clinically, the enhanced diagnostic accuracy provided by combining these modalities can lead to earlier detection of treatment response or resistance, allowing clinicians to promptly adjust treatment plans and reduce unnecessary side effects from ineffective therapies. Moreover, more accurate monitoring of treatment response can help tailor personalized treatment strategies, which is particularly important in recurrent EC, where therapy responses can be highly variable. By leveraging the strengths of both imaging techniques, we can offer more comprehensive and accurate assessments, ultimately improving patient outcomes.

### Disclosure of conflict of interest

None.

# Imaging evaluation of recurrent endometrial cancer

**Address correspondence to:** Xueling Wang, Department of Imaging, Yantaishan Hospital, No. 91 Jiefang Road, Zhifu District, Yantai 264001, Shandong, China. E-mail: ytsyywxl@163.com

## References

- [1] Yue X, He X, He S, Wu J, Fan W, Zhang H and Wang C. Multiparametric magnetic resonance imaging-based radiomics nomogram for predicting tumor grade in endometrial cancer. *Front Oncol* 2023; 13: 1081134.
- [2] Yu Y, Zhang L, Sultana B, Wang B and Sun H. Diagnostic value of integrated (18)F-FDG PET/MRI for staging of endometrial carcinoma: comparison with PET/CT. *BMC Cancer* 2022; 22: 947.
- [3] Ytre-Hauge S, Salvesen ØO, Krakstad C, Trovik J and Haldorsen IS. Tumour texture features from preoperative CT predict high-risk disease in endometrial cancer. *Clin Radiol* 2021; 76: 79.e13-79.e20.
- [4] Yoshida M, Saida T, Mori K, Hoshiai S, Sakai M, Amano T, Shibuki S, Miyata M, Sato T and Nakajima T. Comparison of preoperative diagnostic performance between dual-energy CT, conventional CT, and MRI in endometrial cancer. *Pol J Radiol* 2024; 89: e358-e367.
- [5] Winarto H, Habiburrahman M, Siregar TP and Nuryanto KH. Magnetic resonance imaging pitfalls in determining myometrial invasion in stage I endometrial cancer: a case report and literature review. *Radiol Case Rep* 2022; 17: 2680-2688.
- [6] Weissinger M, Bala L, Brucker SY, Kommos S, Hoffmann S, Seith F, Nikolaou K, la Fougère C, Walter CB and Dittmann H. Additional value of FDG-PET/MRI complementary to sentinel lymph node staging in patients with endometrial cancer: a prospective study. *Diagnostics (Basel)* 2024; 14: 376.
- [7] Wang X and Zhang R. Clinical value analysis of combined vaginal ultrasound, magnetic resonance dispersion weighted imaging, and multi-layer spiral CT in the diagnosis of endometrial cancer using deep VGG-16 AdaBoost hybrid classifier. *J Oncol* 2022; 2022: 7677004.
- [8] Tsuyoshi H, Tsujikawa T, Yamada S, Okazawa H and Yoshida Y. Diagnostic value of (18)F-FDG PET/MRI for staging in patients with endometrial cancer. *Cancer Imaging* 2020; 20: 75.
- [9] Terada N, Matsuura M, Kurokawa S, Teramoto M, Hanakenaka M and Saito T. Comparative evaluation of preoperative imaging and post-operative histopathology in 108 patients who underwent laparoscopic- or robot-assisted surgery for endometrial cancer. *Gynecol Minim Invasive Ther* 2022; 11: 203-208.
- [10] Tarcha Z, Konstantinoff KS, Ince S, Fraum TJ, Sadowski EA, Bhosale PR, Derenoncourt PR, Zulfiqar M, Shetty AS, Ponisio MR, Mhlanga JC and Itani M. Added value of FDG PET/MRI in gynecologic oncology: a pictorial review. *Radiographics* 2023; 43: e230006.
- [11] Suzuki S, Kurokawa R, Tsuruga T, Mori-Uchino M, Nishida H, Kato T, Abe H, Ushiku T, Amemiya S, Katayama A and Abe O. CT, MRI, and FDG-PET imaging findings of low-grade extrauterine endometrial stromal sarcoma arising from the mesentery: a case report. *Radiol Case Rep* 2021; 16: 2774-2779.
- [12] Silva C, Carneiro C and Cunha TM. Role of imaging in the management of high-risk endometrial cancer. *Cureus* 2021; 13: e19286.
- [13] Sertic M, Kilcoyne A, Catalano OA and Lee SI. Quantitative imaging of uterine cancers with diffusion-weighted MRI and 18-fluorodeoxyglucose PET/CT. *Abdom Radiol (NY)* 2022; 47: 3174-3188.
- [14] Schwartz LH, Litière S, de Vries E, Ford R, Gwyther S, Mandrekar S, Shankar L, Bogaerts J, Chen A, Dancey J, Hayes W, Hodi FS, Hoekstra OS, Huang EP, Lin N, Liu Y, Therasse P, Wolchok JD and Seymour L. RECIST 1.1-update and clarification: from the RECIST committee. *Eur J Cancer* 2016; 62: 132-137.
- [15] Berek JS, Matias-Guiu X, Creutzberg C, Fotopoulou C, Gaffney D, Kehoe S, Lindemann K, Mutch D and Concin N. FIGO staging of endometrial cancer: 2023. *J Gynecol Oncol* 2023; 34: e85.
- [16] Seban RD, Donnadieu A, Journo G, Bidard FC, Richard C, Rouzier R and Champion L. (18)F-FDG PET/CT in relapsed endometrial cancer treated with preoperative PD-1 inhibitor Dostarlimab. *Diagnostics (Basel)* 2021; 11: 1353.
- [17] Schnarr KL, Seow H, Pond GR, Helpman L, Elit LM, O'Leary E and Kong I. The impact of preoperative imaging on wait times, surgical approach and overall survival in endometrioid endometrial cancers. *Gynecol Oncol* 2022; 165: 317-322.
- [18] Schnarr KL, Seow H, Elit LM, Pond GR, Helpman L, O'Leary E and Kong I. The use of imaging in endometrial cancer prior to potential surgery: are guidelines being followed? *Gynecol Oncol* 2021; 161: 361-366.
- [19] Sallée C, Marguerite F, Gouy S, Tardieu A, Belghiti J, Lambaudie E, Collinet P, Guyon F, Legros M, Monteil J and Gauthier T. FDG-PET/CT and para-aortic staging in endometrial cancer. A French multicentric study. *J Clin Med* 2021; 10: 1746.
- [20] Sadowski EA, Pirasteh A, McMillan AB, Fowler KJ and Kusmirek JE. PET/MR imaging in gynecologic cancer: tips for differentiating normal

## Imaging evaluation of recurrent endometrial cancer

- gynecologic anatomy and benign pathology versus cancer. *Abdom Radiol (NY)* 2022; 47: 3189-3204.
- [21] Rockall AG, Barwick TD, Wilson W, Singh N, Bharwani N, Sohaib A, Nobbenhuis M, Warbey V, Miquel M, Koh DM, De Paepe KN, Martin-Hirsch P, Ghaem-Maghani S, Fotopoulou C, Stringfellow H, Sundar S, Manchanda R, Sahdev A, Hackshaw A and Cook GJ. Diagnostic accuracy of FEC-PET/CT, FDG-PET/CT, and diffusion-weighted MRI in detection of nodal metastases in surgically treated endometrial and cervical carcinoma. *Clin Cancer Res* 2021; 27: 6457-6466.
- [22] Nordskar NJ, Hagen B, Ogarkov A, Vesterfjell EV, Salvesen Ø and Aune G. Initial experience with positron emission tomography/computed tomography in addition to computed tomography and magnetic resonance imaging in preoperative risk assessment of endometrial cancer patients. *Eur J Obstet Gynecol Reprod Biol* 2021; 259: 46-52.
- [23] Mohammadinejad P, Kim A, Koshevarova V, Murphy M, Shagun F and Bhargava P. Synchronous endometrial cancer detected on 68 Ga-DOTATATE PET/CT. *Clin Nucl Med* 2024; 49: 96-97.
- [24] Li C, Yu J and Fu Z. Application of CT and MRI combined with VEGF-C and EGFR in the identification of endometrial cancer stages. *Am J Transl Res* 2021; 13: 7164-7171.
- [25] Larson M, Lovrec P, Sadowski EA and Pirasteh A. PET/MRI in gynecologic malignancy. *Radiol Clin North Am* 2023; 61: 713-723.
- [26] Kunikowska J, Pełka K, Bizoń M and Olszewski M. 68Ga-prostate-specific membrane antigen PET/CT in endometrial cancer: a preliminary report. *Clin Nucl Med* 2024; 49: e650-e655.
- [27] Kido A, Himoto Y, Kurata Y, Minamiguchi S and Nakamoto Y. Preoperative imaging evaluation of endometrial cancer in FIGO 2023. *J Magn Reson Imaging* 2024; 60: 1225-1242.
- [28] Sala E, Kataoka MY, Priest AN, Gill AB, McLean MA, Joubert I, Graves MJ, Crawford RA, Jimenez-Linan M, Earl HM, Hodgkin C, Griffiths JR, Lomas DJ and Brenton JD. Advanced ovarian cancer: multiparametric MR imaging demonstrates response- and metastasis-specific effects. *Radiology* 2012; 263: 149-159.
- [29] Lee SW, Jeong SY, Kim K and Kim SJ. Direct comparison of F-18 FDG PET/CT and MRI to predict pathologic response to neoadjuvant treatment in locally advanced rectal cancer: a meta-analysis. *Ann Nucl Med* 2021; 35: 1038-1047.
- [30] Hoffman RM, Atallah RP, Struble RD and Badgett RG. Lung cancer screening with Low-Dose CT: a meta-analysis. *J Gen Intern Med* 2020; 35: 3015-3025.
- [31] Kidd EA. Imaging to optimize gynecological radiation oncology. *Int J Gynecol Cancer* 2022; 32: 358-365.
- [32] Hashimoto C, Shigeta S, Shimada M, Shibuya Y, Ishibashi M, Kageyama S, Sato T, Tokunaga H, Takase K and Yaegashi N. Diagnostic performance of preoperative imaging in endometrial cancer. *Curr Oncol* 2023; 30: 8233-8244.
- [33] Fasmer KE, Gulati A, Dybvik JA, Ytre-Hauge S, Salvesen Ø, Trovik J, Krakstad C and Haldorsen IS. Preoperative 18F-FDG PET/CT tumor markers outperform MRI-based markers for the prediction of lymph node metastases in primary endometrial cancer. *Eur Radiol* 2020; 30: 2443-2453.
- [34] Fasmer KE, Gulati A, Dybvik JA, Wagner-Larsen KS, Lura N, Salvesen Ø, Forsse D, Trovik J, Pijnenborg JMA, Krakstad C and Haldorsen IS. Preoperative pelvic MRI and 2-[(18)F]FDG PET/CT for lymph node staging and prognostication in endometrial cancer-time to revisit current imaging guidelines? *Eur Radiol* 2023; 33: 221-232.